Cost-effective carbon fiber precursor selections of polyacrylonitrile-derived blend polymers: carbonization chemistry and structural characterizations

Qian Mao,[a] Siavash Rajabpour,[b] Mahdi Khajeh Talkhoncheh,[b] Jiadeng Zhu,[c] Malgorzata Kowalik[a] and Adri C. T. van Duin[a,b]

[a]Department of Mechanical Engineering, The Pennsylvania State University, University Park, PA, 16802, USA.
[b]Department of Chemical Engineering, The Pennsylvania State University, University Park, PA, 16802, USA
[c]Chemical Sciences Division, Oak Ridge National Laboratory, Oak Ridge, TN, 37831, USA

Blending polyacrylonitrile (PAN) with plastic wastes and bio-based polymers provides a convenient and inexpensive method to realize cost-effective carbon fiber (CF) precursors. In this work, PAN-based blend precursors are investigated using ReaxFF reactive molecular dynamics simulations with respect to the formation of all-carbon rings, the evolutions of oxygen-containing and nitrogen-containing species, and the migration of carbon atoms to form turbostratic graphene. From these simulations, we identify that PAN/ cellulose (CL) blend manifests the highest carbon yield and the most substantial all-carbon ring formation. This ReaxFF-based finding is confirmed by Raman and TEM experiments indicating high crystallinity for PAN/CL-derived blend CFs. We trace the pathway of gasification and carbonization of PAN/CL to elaborate the mechanism of the formation of all-carbon ring networks. We discover that the acetals of CL can catalyze the cyclization of the blend precursor, allowing for the search for CL derivatives or the other kinds of bio-based polymers with similar functionalities as alternative blends. In addition, we examine the structural characteristics using the carbon–carbon (C–C) radial distribution functions, C–C bond length distributions, and sp^2 C atom ratios for the four representative precursors, *i.e.*, PAN, oxidized PAN, PAN/ nylon 6,6, and PAN/CL. Our simulation results show the most extensive all-carbon ring cluster and graphitic structure growths for PAN/CL. Therefore, we propose PAN/CL as a cost-effective alternative CF precursor, since (a) CL is naturally abundant and eco-friendly for production, (b) the blend precursor PAN/CL does not require oxidation treatment, (c) PAN/CL has a high carbon yield with substantial all-carbon ring formation, and (d) PAN/CL based CFs potentially provide a mechanical property enhancement.

1. Introduction

Recently, global warming and energy crises have increased the interest in high-strength polyacrylonitrile (PAN)-based carbon fibers (CFs) as super-light materials for raising energy efficiencies. PAN-based CFs demonstrate good performance in extreme environments[1] due to their unique properties, such as high strength-to-weight ratio, high tensile modulus and tensile strength, and superior chemical stabilities.[2,3] These remarkable properties make PAN-based CFs a versatile reinforcing material in aerospace, military, automotive industry, and sporting goods.[4,5] However, a high cost of PAN-based CF production has greatly limited the application of such precursors in worldwide markets,[6] specifically, more than 50% of the cost is related to the production of precursor fibers.[7] Thus, the key to reducing the cost of CF production is to employ alternative precursors, ideally eliminating the oxidation process.

Alternative CF precursors, considered as recycled plastics and fibers or natural waste byproducts,[8] such as polyethylene terephthalate (PET),[9–11] polyolefins,[12,13] nylon,[14,15] rayon,[16,17] lignin,[18–20] and cellulosic biomass,[21,22] *etc*., have been widely reported, even though the resultant alternative CFs may not sustain the same mechanical properties as those from PAN-based CFs. For instance, the recycled plastics such as the two common polyolefins,[23] polyethylene (PE) and polypropylene (PP), can substantially decrease the cost of CF production.[24] However, direct carbonization of polyolefins does not generate a char-like carbon residue, because they melt at a relatively low temperature and become short-chain hydrocarbons or gaseous products.[25,26] Therefore, these precursors are typically functionalized and cross-linked prior to the high temperature carbonization by means of sulfonation,[27–29] where oxygen (O)- and sulfur (S)-containing groups play a critical role in the chemical transformations of dehydrogenation, crosslinking, and carbonization.[30,31] On the other hand, the utilization of O-containing polymers such as poly(p-phenylene-2,6-benzobisoxazole (PBO) has been identified to effectively eliminate high-cost oxidation process in traditional CF conversion,[32–34] thus making the carbonization process more energy- and time-saving along with high-performance CF yield.[35–38] Nevertheless, PBO-based CFs are still quite expensive due to few demands in the market. Thus, to reduce the total cost, there is always a delicate balance between the selection of CF precursors and the development of O-/S-functionalization and carbonization protocols for these polymers. In addition, despite impurity and defects as well as high emission of gaseous species generated by bio-based precursors,[22,39,40] there still has been growing interest in the development of various kinds of bio-based polymers as CF precursors, including cellulose (CL), hemicellulose, lignin, *etc*., attributed to their natural abundance, renewable properties, low environmental impact, and low cost.[41–44]

Inspired by the previous discussion, polymer blending has been considered as a convenient and economical way to develop novel alternative CF precursors.[9] The application of PAN-based blending is to introduce O-containing groups that significantly accelerate[45] or possibly eliminate[34] the oxidation process for PAN. With proper spinning techniques, the mechanical properties of the resultant CFs can be well-sustained.[19,46,47] For example, Dong *et al*.[48] reported that the Young's modulus and tensile strength of PAN/lignin sulfonate (LS) blend CFs decayed as the LS content increased, whereas when the dope concentration of acrylonitrile/itaconic acid increased, the fiber structural and mechanical properties were

improved as a result of the finger-like pore elimination through the doping. Jin *et al*.[49] measured the Young's modulus and tensile strength of an equi-component (1:1 in weight ratio) PAN/lignin blend CF as high as 130 ± 3 GPa and 1.2 ± 0.1 GPa respectively, although larger disordered graphitic structure was observed resulting from lignin. Tay *et al*.[50] synthesized a superior PAN/resorcinol-based phthalonitrile prepolymer (pPN) CF precursor, from which the enhanced thermal stability and the carbonaceous material with lower shrinkages and significantly enhanced carbon yield and mechanical properties than the pristine samples were obtained. In addition, other chemical modification methods for preparing PAN-based composite CF precursors such as polymer doping (low amount polymer integration to PAN),[51] copolymerization,[52] surface coating,[53] *etc*. have also been utilized to optimize the processing conditions and improve the structural and mechanical properties for low-cost PAN-based CF production.

From the above literature, introducing polymers with various functionalities to PAN has become a mainstream of tuning materials and mechanical properties as well as developing cost-effective PAN-based CF precursors. In our previous work,[34] we proposed PAN/PBO blends as a cost-effective CF precursor, from which we also elucidated the role of O-containing groups in the blends as to efficiently initiating the carbonization process, and the role of N-containing groups as to capturing and converting carbon radical species into the graphitic networks in the subsequent carbonization process. Since the all-carbon ring structure yield was as competitive as pure PBO or oxidized PAN, and the oxidation process was no longer required, the PAN/PBO blends could effectively reduce the cost of CF production. However, as we mentioned earlier, the cost of PBO is still quite high in the current market. Herein, we further propose three inexpensive polymers, PET, nylon 6,6, and CL, blended with PAN, for the development of alternative PAN-based blend CF precursors.

In this study, we first apply the ReaxFF C/H/O/N-2019 force field[54] to investigate the all-carbon ring structure formation together with the evolutions of O- and N-containing groups, and then we delve deeper into the atomistic structural analyses as well as the carbon–carbon (C–C) bond hybridization to characterize the crystallinity of the all-carbon ring networks. From there, we select the PAN-based blend precursor that gives the best performance for producing high carbon yield yet at low cost. Lastly, we employ the experimental approach to qualitatively substantiate our atomistic findings. Our analyses provide the atomistic insights into the carbonization mechanism of the PAN-based blend precursors, and it could also guide the understanding of the potential mechanical property enhancement for industrial applications.

2. Simulation and experimental methods

2.1 ReaxFF MD simulations

2.1.1. ReaxFF method. To understand the atomistic details of blending PAN with various polymers, we performed reactive molecular dynamics (MD) simulations using the ReaxFF method. ReaxFF is a bond order based empirical force field, which employs a continuous function with respect to bond order and bond distance for the bonded interactions and van der Waals and Coulomb terms for the nonbonded interactions.[55,56] The continuous functions are

parametrized against the quantum mechanics (QM) or experimental data, allowing for the ReaxFF simulations on significantly larger systems than QM-based methods with comparable accuracy. As such, the ReaxFF method has been widely used to investigate the chemistry of large carbon systems, such as pyrolysis and combustion of carbonaceous compounds,[57–61] oxidation of hydrocarbons,[62–65] and graphitization of carbon fiber precursors.[34,54,66,67]

In this work, we implement the ReaxFF C/H/O/N-2019 force field parameters[54] to simulate the carbonization process of PAN-based blend precursors, with a focus on the carbonization chemistry for various O-containing polymers reacting with PAN as well as their structural characterizations associated with the crystallography and the predictions for mechanical properties. In this force field, the triple bond stabilization energy term is integrated to make the N_2 molecules adequately stable and not react with the carbon radicals at high temperature, so that the frequent gas removal of N_2 during the carbonization is not required. This force field has been successfully utilized to simulate a wide range of O- and N-containing polymer precursors, which its validity has also been substantiated by the experimental work.[33,68,69]

2.1.2. ReaxFF MD simulation procedure. We performed a series of ReaxFF MD simulations on single and PAN-based blend precursors (Fig. 1), to mimic the carbonization process and search for the superior candidate that can reduce the total cost of CF production. Besides the modeling of single precursors, *i.e.*, PAN, PBO, the proposed oxidized PAN,[66,70] the CL extracted from a CL Iβ crystal,[71,72] PET, nylon 6,6, the PAN-based blend precursors were built by blending PAN with the above polymers with a molar ratio of 1:1. The molar ratio of 1:1 used here is to reflect a representative high content of these polymers being incorporated into PAN matrix, from which inexpensive or abundant polymers could be extensively exploited and effectively substitute for PAN. Recent research has shown that high contents of biomolecules, *i.e.*, 25 wt%– 85 wt%,[49,73,74] can be applied with unaffected spinnability for fabricating PAN-based blend CFs if the processing conditions are delicately optimized. In the following text, we will use the names PAN, PBO, oxidized PAN, CL, PET, nylon for the above single polymers for short. The molecular chain length was adjusted to ensure that the total carbon (C) atom number of each polymer was around 50, and then 50 molecules of single or blend precursors were randomly placed in an orthogonal simulation box as a starting point. After performing the energy minimization for these ten precursors, we compressed the orthogonal simulation boxes triaxially with a strain rate of -0.02 ps^{-1} from the initial density of 0.08–0.21 g cm^{-3} to the final density of 1.60 g cm^{-3}, which was within the range of 1.2–2.0 g cm^{-3} during the PAN-based CF production.[70,75] Afterwards, we equilibrated the system at 300 K with NVT ensemble for 300–1000 ps to ensure the convergence of the potential energy. Periodic boundary condition was applied to all three directions of the orthogonal simulation box, the time-step was set to be 0.25 fs, and the bond order of the molecule identification was set to be 0.3. The thermal oxidative stabilization at 200–300 °C is a critical step for many kinds of PAN-based CF precursors undergoing oxidation, dehydrogenation, cyclization which allow further carbonization at a temperature above 1000 °C.[76,77] Nevertheless, the stabilization process is the most energy consuming and time expensive stage in the manufacture of CFs.[78–80] Thus, in this research, we aim to bypass the conventional oxidation process prior to carbonization and produce alternative CF precursors in an energy-saving manner. As such, we employ the direct carbonization in both the experiment and ReaxFF simulations. Accordingly, each system was heated up from 300

K to 2800 K with a heating rate of 10 K ps^{-1}, as shown in Fig. S1. We defined t = 0 ps as the point where the heating starts, for precursors should undergo the inception of thermal decomposition during the heating step. The standard carbonization of the single and blend precursors was carried out at 2800 K in NVT ensemble for 2000 ps (up to t = 2250 ps in Fig. S1). However, in order to better characterize the structural distinctions of the representative precursors of our interest, i.e., PAN, oxidized PAN, PAN/CL, and PAN/nylon, the extended carbonization for another 6000 ps was applied (up to t = 8250 ps in Fig. S1). The six configurations, represented by different coordinates and velocities, were saved every 10 ps prior to the standard carbonization. Afterwards, these configurations were submitted to the standard carbonization running for 2000 ps separately, then we obtained six distinct samples of each precursor for the statistical calculations. To investigate the temperature effect on the carbonization process, we considered the oxidized PAN samples heated from 300 K to 2200 K, 2500 K, and 2800 K with a heating rate of 10 K ps^{-1}. These simulation data were further compared with the experimental results.

The methods of performing data analyses and data presentations for the figures presented in the main manuscript can be found in section S1: data postprocessing details in ESI, and those for the comparative study on oxidized PAN under-going carbonization at elevated temperatures can be found in section S2: morphological variations of carbonized oxidized PAN from experiment and ReaxFF simulations in ESI.

2.2. Experimental procedure

2.2.1. Materials. PAN (powder, average M_w = 150 000), CL (powder, a particle size of 25 μm), nylon 6,6 (pellets, M_w = 262.35), dimethyl sulfoxide (DMSO) (anhydrous, ≥99.9%), and formic acid (HPLC, ≥99%, M_w = 78.13) were purchased from Macklin. Both the as-spun PAN and oxidized PAN fibers were received from Bluestar Fibers, Co. Ltd. All the materials were used without any purification.

2.2.2. Preparation of oxidized PAN CFs, PAN, PAN/cellulose, PAN/nylon derived carbon materials. The as-received oxidized PAN fibers were carbonized at 700 °C, 900 °C, and 1500 °C, respectively, for 30 min with a heating rate of 5 °C min^{-1} under a N_2 atmosphere, and then they were cooled down to room temperature.[68] For the PAN/CL blend, PAN and CL, with a 1:1 molar ratio of molecules, were dissolved and dispersed in DMSO *via* magnetic stirring to form a uniform suspension followed by putting the above suspension into a vacuum oven at 80 °C overnight to remove DMSO. And for the PAN/nylon blend, with a 1:1 molar ratio of molecules, nylon was first dissolved in formic acid. Then, the PAN powder with equivalent molecules to nylon was added to the solution with the assistance of stirring. Finally, formic acid was evaporated by the vacuum oven at 60 °C. In the carbonization step, the PAN, PAN/cellulose, and PAN/nylon were directly carbonized at 1500 °C for 30 min with a heating rate of 5 °C min^{-1} under a N_2 atmosphere.

2.2.3. Characterization. The micro-structure of prepared carbon materials was investigated by high-resolution transmission electron microscopy (HR-TEM, FEI Titan) and Raman spectroscopy equipped with a 514 nm laser beam (Renishaw InVia).

3. Results and discussion

3.1. All-carbon ring formation for all precursors

In our previous work,[34] we have identified that the PAN/PBO blend with a molar ratio of 1:1 can give comparable amount of 6-membered all-carbon ring formation with PBO or oxidized PAN, and its conversion rate is considerably fast as well. In this work, we aim to explore the lower-cost alternative for the PAN-based blend precursors with comparable 6-membered all-carbon ring production. Herein, we further consider the inexpensive O-containing polymers, CL, PET, and nylon as a component, as shown in Fig. 1(d–f), for the PAN-based blend precursors.

In Fig. 2, we normalize the conversion ratios of C atoms to 5,6,7-membered all-carbon rings for the ten precursors during the last 1000 ps of carbonization (from t = 1250 ps to t = 2250 ps). The first column (Fig. 2(a–c)) shows the all-carbon ring formation of the four precursors discussed in our previous work,[34] and the second column (Fig. 2(d–f)) demonstrates the all-carbon ring formation of the three inexpensive single precursors proposed in this work, followed by the plots of the PAN-based blend precursors, PAN/CL, PAN/PET, and PAN/nylon in the third column (Fig. 2(g–i)). The profiles of the C conversion ratios to 5,6,7-membered all-carbon rings of all considered precursors, inclusive of both heating and carbonization processes, can be seen in Fig. S2(a–c).

In Fig. 2, PAN/CL and PAN/PET present the highest conversion ratios to 6-membered rings (nearly 0.8) at the end of carbonization, even higher than the PAN/PBO from our previous work[34] by around 0.1. The rest precursors, except nylon and PAN/nylon, exhibit higher conversion ratios of 5,6,7-membered all-carbon rings than the single PAN precursor. This suggests that O-containing groups with single C–O bonds are efficient for initiating carbonization process and responsible for the growth of all-carbon ring clusters, which is in accordance with our previous study.[34] However, both nylon and PAN/nylon blend precursors display the lowest conversion ratios to 6-membered all-carbon rings, thus they should not be considered as cost-effective CF precursors, despite that nylon is typically much cheaper than PAN. The conversion ratios of 5,6,7-memebred all-carbon rings for the ten precursors at 250 ps and at 2250 ps can be seen in Fig. S3(a) and (b). It should be noted that the initial high conversion ratios of 6-membered all-carbon rings from PBO, PAN/PBO, PET, and PAN/PET in Fig. S3(a) result from the benzene ring-like structures in PBO and PET molecules. Whereas the conversion ratios to 6-membered all-carbon rings in Fig. S3(b) result from the graphene-like structures, which implicates that the precursors initially having benzene ring-like structures undergo all-carbon ring opening, reorganization and cyclization.

U.S. Department of Energy studies have identified that fossil-based PAN CFs are the most promising materials for the light-weight vehicles, offering as much as 60% weight reduction, but at up to ten times the cost.[81] The manufacturing cost of CFs is highly dependent on oil price, with around 51% being precursor cost, 18% utilities, 12% depreciation, 10% labor and 9% represented by other fixed costs.[82] This motivates the development of cost-effective CF precursors, preferably from renewable alternatives.[83] Lignin and cellulose are two interesting candidates as sources for CF because they are renewable macromolecules available in high

quantities.[84,85] The high demands for PAN-based CFs lead governments around the world to promulgate laws on the reuse and recycling of the materials.[86] In the meantime, researchers around the world have carried out extensive developmental research towards making PAN-based precursors greener and partially replacing PAN with a renewable resource for manufacturing eco-friendly CF precursors.[49,87–90] Based on the data discussed earlier, where we see a comparable all-carbon ring conversion ratio of PAN/CL with that of PBO, oxidized PAN, or PAN/PBO, as well as the fact that CL is an economical and eco-friendly polymer among all the candidates, we propose PAN/ CL as a cost-effective alternative for PAN-based blend CF precursors. To further investigate PAN-based blend precursors with the best and the least performance, we select PAN/CL and PAN/nylon, together with the comparative precursors, PAN and oxidized PAN, for the representative precursors of interest. The structural characterizations of these four representative precursors will be detailed in section 3.4. Additionally, in Fig. S3(c), we calculate the ratios

$$R_{\frac{\text{6-MR}}{\text{5-MR \& 7-MR}}}$$

to examine the dominance of 6-membered all-carbon rings over 5- and 7-membered all-carbon rings, corresponding to topological defects in graphitic structures. Although PAN/CL and PAN/PET have the highest conversion ratios of 6-membered all-carbon rings, they exhibit slightly lower

$$R_{\frac{\text{6-MR}}{\text{5-MR \& 7-MR}}}$$

ratios than PAN, oxidized PAN, and 5-MR & 7-MR PAN/PBO. In other words, more extensive growth of all-carbon ring clusters occurs during the carbonization of PAN/CL and PAN/PET, yet the clusters may be less graphitized than PAN, oxidized PAN, and PAN/PBO as the carbonization time is prolonged. However, the presence of 5- and 7-membered all-carbon rings should not be the only parameter that affects the mechanical properties of the resultant CFs.[91]

3.2. Turbostratic graphene structure growth and evolutions of O- and N-containing species

During carbonization process, O- and N-containing groups of precursors evolve to mobile radicals and volatile gases, which mobile radicals can move to the interface of other polymer segments and initiate the cyclization of carbon radicals. Afterwards, the emission of volatile gases facilitates the spontaneous cyclization of the adjacent carbon radicals. The evolutions of normalized O- and N-containing gases and groups in percentage during heating and carbonization (from $t = 0$ ps to $t = 2250$ ps) are presented in Fig. 3(a–d).

The emission of O- and N-containing gases leads to the reduction of O- and N-containing groups. The O-containing groups decay dramatically as the carbonization starts, converting to the O-containing gases with a deep slope in curves, as shown in Fig. 3(a and b). On the contrary, the N-containing groups decrease much more slowly, evolving to the N-containing gases with a gentle slope in curves, as shown in Fig. 3(c) and (d). These observations are in good agreement with the experiments.[32,92] Although as can be seen in Fig. 3(a) and (b), the conversions of O-containing groups of CL and PAN/CL to O-containing gases shows little difference from other precursors, the ratios of remaining O-containing species of CL and

PAN/CL are significantly higher due to the higher amount of O atoms from CL, as shown in Fig. 3(e). Unlike O-containing groups that are more efficient for initiating the carbonization, the role of the remaining N-containing groups is to assist the further growth of all-carbon ring clusters and the formation of graphitic structures. However, excess of N-containing groups may lead to low carbon yield, and the slow conversion rate would increase the energy consumption in real applications. In Fig. 3(c) and (d), PBO shows the slowest conversion rate from N-containing groups to N-containing gases, yet the ratios of its remaining N-containing species are relatively lower than PAN, oxidized PAN, and PAN/PBO, as shown in Fig. 3(f), thus making it possible to generate relatively higher amount of 6-membered all-carbon rings at the end of carbonization (t = 2250 ps).

The mass percentage of volatile gases is another measure for evaluating the carbonization reaction for the ten precursors. The mass percentages of commonly observed gases of small molecular weight, CH_4, CO, CO_2, H_2, H_2O, N_2, NH_3, are presented in Fig. S4(a–g), and the total mass percentages of the above gases are summed in Fig. S4(h). There are also other types of small gas molecules or radicals (M_w <50 g mol^{-1}) not being counted, for they appear sporadically in the MD trajectories, accounting for less than 3 wt%. Interestingly, the carbonization of PAN-based blend precursors typically reduces the emissions of C-containing gases (CH_4, CO, CO_2), compared with those from the associated single polymer precursors. For instance, the carbonization of a single CL precursor generates over 20 wt% of CO_2, whereas the carbonization of the PAN/CL blend precursor reduces the CO_2 yield to ~2.5 wt%, which means the PAN/CL precursor enables more carbon residues to retain in the system for the subsequent carbonization, other than leaving all-carbon ring and graphitic networks as volatile gases. Analogously, the total mass percentages of the volatile gases decrease when using the PAN-based blend polymers as CF precursors. Taking CL and PAN/CL as an example, the average total gas mass percentage for the carbonized single CL precursor can be as high as 57.2 ± 0.7 wt%, while for the carbonized PAN/CL blend precursor, this value decreases to 41.1 ± 0.6 wt%. Considering the total mass percentages of hetero elements (elements excluding C) for CL and PAN/CL systems are 56.1 wt% and 46.7 wt%, there are about 1.1 wt% carbon from CL going away at the end of the carbonization (t = 2250 ps), whereas about 5.6 wt% hetero elements retained in the PAN/CL system, assisting the further carbonization as the elapsed time is prolonged. Namely, blending CL with PAN could help retain more heteroatoms in the system, hence a better chance of the growth and propagation of graphitic structures. The total gas mass percentages and hetero element mass percentages for the ten single and blend precursors are tabulated in Table S1. From the table, CL and PET are the only two single precursors that have higher gas mass percentages than the hetero element mass percentages. However, with the introduction of PAN to CL and PET as blends, the gas emissions can be significantly decreased.

In order to trace the growth of all-carbon rings, we evaluate the carbon conversion to C atoms either in the basal plane or on the edges of turbostratic graphene at the end of carbonization (t = 2250 ps), as shown in Fig. 4(a) and (b). The oxygen and nitrogen conversions of commonly observed O- and N-containing groups are profiled as well, as shown in Fig. 4(c–e).

In Fig. 4(a), PAN-based blends exhibit a significant increase in the basal plane C conversion, except PAN/PBO, compared to the individual single precursors. Particularly, PAN/CL

demonstrates the highest conversion of C atoms growing in the basal plane (~77.7 ± 0.9%), followed by PAN/PET (~76.7 ± 1.2%), while PAN/nylon is at the bottom of the PAN-based blend precursors (63.5 ± 2.3%). The percentages of C atoms growing on edges are approximately the same for the ten precursors, suggesting that the peripheral length of turbostratic graphene for all considered cases are of small difference, yet the transformation of undercoordinated and amorphous C atoms to the basal plane C atoms of turbostratic graphene prevails the carbonization process. The ratios of basal plane C atoms presented in Fig. 4(b) demonstrate a subtle difference among precursors. For example, nylon exhibits a ratio of basal plane C atoms comparable to the ratio of PAN/nylon, *i.e.*, for both nylon and PAN/nylon, about 83% C atoms transform to basal plane C atoms, although nylon possesses a fewer number of C atoms constituting 3 to 8-membered all-carbon rings than PAN/nylon. All O-containing groups for the ten precursors decay to less than 4%, as shown in Fig. 4(c), whereas as can been seen in Fig. 4(e) and (f), there are a substantial number of N-containing groups not converting to gas molecules. In Fig. 4(f), among the four PAN-based blend precursors, PAN/CL shows the least ratios of remaining N-containing groups, which gives rise to more substantial formation of all-carbon rings than the other precursors. Recall that the remaining N-containing groups would retain in all-carbon ring networks for longer time, manifesting slower transformation of C atoms to the basal plane. Furthermore, the excessive remaining graphitic-N groups may prevent carbon radicals and polymer residues from converting to turbostratic graphene or graphitic networks, due to the presence of heteroatoms in all-carbon rings. PAN/nylon has the least ratio of graphitic-N groups among all PAN-based precursors; however, as its O- and N-containing groups are burned out into volatile gases in the early stage of carbonization, it has a smaller chance of producing extensive all-carbon ring structures than PAN/CL does. The rest of remaining N-containing groups of PAN/nylon could continue to capture and convert carbon radical species into all-carbon ring networks, yet at a very low reaction rate.

3.3. The transformation of PAN and PAN-based blend polymers to all-carbon rings

From the above analyses, we identify the evolution of all-carbon rings in response to the transformations of O- and N-containing species. In the meantime, we demonstrate that blending O-containing polymers with PAN places the PAN-based blends the superior precursors to single O-containing polymers in terms of the performance of all-carbon ring formation. However, the chemical pathway of how PAN from PAN-based blends could yield more all-carbon rings is not yet well understood.

Herein, we plot the ratios of C atoms either coming from PAN or coming from the blended polymers as they form all-carbon ring structures at the end of carbonization (t = 2250 ps), as shown in Fig. 5(a and b). The transparent and solid bars represent the ratio contributions from PAN and from the blended polymers. Analogous to the results shown in Fig. 2, PAN/CL displays the highest C conversion ratios to 3 to 8-membered (Fig. 5(a)) and to 6-membered (Fig. 5(b)) all-carbon rings. Moreover, PAN/CL has higher ratio of C atoms from PAN converting to all-carbon rings than PAN/PBO does.

To better rationalize the role of PAN in converting PAN-based blend polymers to all-carbon ring structures, we present the atomistic schematics in Fig. 5(c and d) to elaborate the all-

carbon ring growth mechanisms for PAN/PBO and PAN/CL blends. In Fig. 5(c), an O connects with two C atoms, C_1 and C_2, as a bridge bond, at t = 0 ps. The cleavage of C–O–C occurs immediately as the heating step starts, then the O atom goes away and becomes hydrogenated, converting to an H_2O gas molecule. At t = 316 ps, the undercoordinated C_1 bonds with the carbon radicals from PAN and PBO chains in the vicinity, whereas C_2 stays with its original 6-membered ring. At t = 322 ps, C_1 becomes part of a 12-membered ring, whereas C_2 continues to steadily stay with its original 6-membered ring. Having experienced the cyclization and the rearrangement of all-carbon rings, C_1 connects with three C atoms coming from PBO and forms the edge of a 6-membered all-carbon ring; meanwhile, C_2 also connects with three C atoms originated from PBO, yet it contributes to the formation of graphene basal plane with a 6-membered and a 7-membered all-carbon rings at t = 2250 ps. In Fig. 5(d), the acetal in a glucose ring of CL goes along a distinct pathway than the O-containing group in a benzoxazole ring of PBO, as shown in Fig. 5(c). At t = 0 ps, O_1 and O_2 construct an acetal in a CL molecule, where O_1 binding with C_1 and C_2 is from a glucose ring, and O_2 and C_2 form a glycosidic bond of the glucose ring and a ring-opened radical. The cleavage of C–O bonds happens between C_1–O_1 and C_2–O_2 bonds in turn, afterwards C_2–O_1 completely emits from the CL chain as a CO gas molecule at t = 287 ps. This is different from H_2O emission of the PAN/PBO system as indicated in Fig. 5(c), where the C atoms from PAN/PBO would be less likely to transfer the carbon radicals from PAN to all-carbon ring networks. At t = 288 ps, C_1 begins to bond with three C atoms, with one C atom coming from PAN and two C atoms coming from CL. In the meantime, the C_2–O_1 gas moves to the other place, having the reaction with C radicals. At t = 899 ps, O_1 from C_2–O_1 gas becomes hydrogenated and evolves to an H_2O gas molecule, and C_2 from C_2–O_1 gas deposits on the surface of carbon networks. At t = 900 ps, C_2 connects with two C atoms from PAN and CL and forms a 6-membered all-carbon ring. At t = 2250 ps, both C_1 and C_2 become the basal plane C atoms of turbostratic graphene. Unlike the C_1 and C_2 atoms in Fig. 5(c) that are only connected with the C atoms originated from PBO, the C_1 and C_2 atoms in Fig. 5(d) bond with the C atoms from PAN and CL. In other words, the cleavage of acetals of CL catalyzes the cyclization of carbon radicals and residues from PAN and CL, hence the higher ratio of C contribution from PAN for PAN/CL than for PAN/PBO. Experimental work on the advanced materials derived from PAN/cellulose nanocrystal (CNC) blends has also identified that the activation energy of the PAN cyclization reaction is reduced by the addition of CNC,[93] the thermal stability can be enhanced,[94] and the resultant mechanical properties[47] can be well sustained. We may apply this carbonization pathway drawn from our ReaxFF simulations to the future innovation in screening other bio-based polymers with a similar functional group to CL for converting the renewable polymer source into CF precursors.

3.4. Structural characterizations of representative precursors from experiment and ReaxFF simulations

By comparison with the experimental measurement on the carbonization of oxidized PAN at different temperatures, the ReaxFF C/H/O/N-2019[54] is well suited to the characterization of morphological evolutions of C/H/O/N-based CF precursors undergoing carbonization in a wide range of temperatures.[95,96] The experimental and simulation details can be found in section S2: morphological variations of carbonized oxidized PAN from experiment and ReaxFF simulations in ESI. In this section, we intend to conduct structural characterizations

for the four representative precursors of interest. The carbon content, turbostratic graphene carbon conversion, radial distribution function (RDF), C–C bond length distribution, and sp^2 hybridization of C atoms for PAN, oxidized PA, PAN/CL, PAN/ nylon are detailed in sequence. The objective is to examine the formation of all-carbon rings and the growth of turbostratic graphene structures, and then to identify the possible indication for the mechanical properties of carbonized precursors.

We present the carbon contents and the conversion percentages of turbostratic graphene for the four representative precursors at the end of carbonization (t = 2250 ps) in Fig. 6. The four representative precursors all have considerably high turbostratic graphene carbon conversions (Fig. 6(b)), whereas only PAN/CL exhibits the carbon content as high as ~92% (Fig. 6(a)), reaching the grade of manufacturing CFs.[97] This implicates, PAN/CL has the least heteroatoms in the remaining materials, for the high ratio of O atoms from CL can effectively initiate the carbonization, while the high ratio of H atoms can gasify O- and N-containing compounds as the carbonization gradually proceeds. The carbon content of PAN/nylon is the second highest among the four representative precursors, due to high emissions of O- and N-containing gases shown in Fig. 3(a) and (c). The carbon contents of PAN and oxidized PAN are both below 90%, suggesting significant amounts of O- and N-containing groups still remain in the system.

Next, we compute the C–C pair RDFs, as a function, $g(r)$, of distance, r, for the four representative precursors carbonized at 2800 K over the standard and the extended carbonizations. In Fig. 7(a), the three green dot reference lines, from left to right, correspond to the distances between the target C atom and its 1st, 2nd, and 3rd neighbor C atoms of 1.42 Å, 2.46 Å, and 3.76 Å from a perfect graphene sheet (see the schematic in Fig. S6), denoted as r^{1st}, r^{2nd}, and r^{3rd}, respectively. And the three gray dot reference lines, from left to right, represent the bond lengths of triple bonded, double bonded, and single bonded C–C bonds of 1.20 Å, 1.34 Å, and 1.54 Å, denoted as r^{tb}, r^{db}, and r^{sb}, respectively.

Comparing the locations of peaks with the reference lines enables us to identify the cyclization and growth of turbostratic graphene networks for the four representative precursors. At 250 ps, although the cyclization and the inception of carbonization could happen during the heating step (from t = 0 ps to t = 250 ps), there is no significant difference in the peak intensities of the four representative precursors. As the carbonization proceeds to 2250 ps, the peak intensities of the four representative precursors at r^{1st}, r^{2nd}, and r^{3rd} all increase. The 1st peaks shift leftwards from r^{sb} to r^{1st}, indicating the transformation of C atoms from sp^3 to sp^2 hybridization state, followed by a substantial cyclization. The 2nd peaks that are initially on the right of r^{2nd} shift leftwards as well, and the overlap with r^{2nd} implicates the extensive clustering and growth of turbostratic graphene structures for the four representative precursors. With the carbonization time being prolonged, the turbostratic graphene structures become more crystalized and organized, thus at 8250 ps, the 1st and 2nd peaks appear higher intensities than those at 2250 ps. The increase of the 1st peak intensities signifies higher crystallinity of turbostratic graphene structures, while the increase of the 2nd peak intensities indicates the growth of turbostratic graphene clusters. In Fig. 7(a), among the four precursors carbonized at 2250 ps and 8250 ps, PAN/CL presents the highest crystallinity as it appears the highest 1st peak intensity, and it also yields the biggest cluster of all-carbon

rings as it presents the highest 2nd peak intensity. On the other hand, the 2nd peak of PAN/CL leans more leftwards compared with the other three precursors, corresponding to a higher curvature of the turbostratic graphene networks. Fig. S6 reveals that at 2800 K as the carbonization time is longer than 500 ps ($t \geq$750 ps), the turbostratic graphene structure for the four representative precursors begins to form. The values of the 1st peak locations and intensities for the four representative precursors at 250 ps, 2250 ps, and 8250 ps are tabulated in Table S2. As can be seen from Table S2, when the carbonization takes place for a sufficiently long time, PAN/CL always shows the highest peak intensities than the other precursors. The 1st peak of PAN/nylon primarily occurs at a location close to r^{sb} in the beginning of the carbonization, suggesting no cyclization manifested at the end of heating process, accordingly, it exhibits the lowest 1st peak intensities at 2250 ps and 8250 ps among the four representative precursors.

In order to validate the simulation results, the corresponding experiment is also performed. Fig. 7(b) shows the Raman spectra of the PAN, PAN/CL, and PAN/nylon derived CF precursors carbonized at 1500 °C. All the samples have three characteristic bands at 1356 (D), 1599 (G), and 2800 cm^{-1} (2D), which correspond to defects/disordered regions, ordered graphitic structure, and second-order Raman band, respectively. The three bands indicate the coexistence of amorphous and graphitized carbon. In addition, the degree of the disorder within the carbon structure can be calculated by the ratio of intensities of D band to G band, denoted as I_D/I_G. The I_D/I_G ratios for the PAN, PAN/CL, and PAN/nylon are 1.10, 1.06, and 1.17, as summarized in Table S2. This suggests that PAN/CL has the most ordered structure among all samples, while PAN/ nylon has the most disordered structure – these are in agreement with the ReaxFF MD simulation study.

Furthermore, we obtained the C–C bond length distributions from 6- or 3 to 8-membered all-carbon rings for the four representative precursors to better identify the quality of carbonization, as shown in Fig. 8(a–h). The C–C bond lengths from 6-memebred all-carbon rings (solid color histograms) or from 3 to 8-memebred all-carbon rings (transparent histograms) are assigned to 80 bins from 1.0 Å to 1.8 Å at selected timesteps during carbonization, so that we can trace the transformation of C atoms from amorphous state to graphitized state.

The amorphous structures of precursors before or at the early stage of carbonization comprise C–C bonds in a mixture of a large portion of C–C single bonds and a small portion of C=C double bonds or partial C=C double bonds. When carbonization sufficiently develops, the C–C bond lengths corresponding to the partial C=C bond length of basal plane C atoms in graphene, *i.e.*, r^{1st} of 1.42 Å, turn to dominate. As such, if the C–C bond length concentration of a carbonized precursor occurs at 1.42 Å, then this precursor is more likely to produce highly graphitized all-carbon ring networks. On the other hand, if the C–C bond lengths from 6-membered all-carbon rings of a carbonized precursor account for a larger sum area, then this precursor is expected to yield more extensive turbostratic graphene networks. In Fig. 8(a), (c), (e) and (g), since the 6-membered all-carbon rings can be barely seen in the beginning of carbonization (t = 250 ps), the bars of solid color histograms for the four representative precursors are lower.

The transparent histograms of PAN, PAN/CL, and PAN/ nylon concentrate at ~1.50 Å, indicating a large portion of C–C single bonds; whereas the bond lengths of oxidized PAN concentrate at ~1.45 Å, due to an incomplete decomposition of 6-membered hetero-rings. As the carbonization advances, the solid color and transparent histograms become higher. At 1250 ps, the C–C bond length concentrations of 6-membered all-carbon rings shift towards ~1.42 Å, as shown in Fig. 8(b), (d), (f) and (h). Particularly, PAN/CL demonstrates the highest ratio of solid color area to transparent area in the histograms, implicating the fastest 6-membered all-carbon ring conversion among the four representative precursors. At 2250 ps, the highest bar of PAN/CL from the histogram occurs at 1.42 Å, corresponding to the substantial formation of in-plane graphitic partial C=C bonds, as shown in Fig. S7(c6). However, PAN and PAN/nylon show different bond length concentrations at 2250 ps, which the former locates at ~1.45 Å and the latter manifests a bifurcation at ~1.43 Å and ~1.48 Å, as shown in Fig. S7(a6) and (d6). This indicates that for these two precursors, the 6-membered all-carbon rings form and grow into bigger clusters but the all-carbon ring networks are not well crystalized. When applying the extended carbonization time to the four representative precursors, they present about the same high ratios of solid color area to transparent area in the histograms, as shown in Fig. S7(a7–d7), meaning the 6-membered all-carbon rings dominate in the networks at 8250 ps.

In order to further quantify the crystallization of all-carbon ring structures for the four representative precursors, we calculate the sp^2 C ratios with two methods, as detailed in Section S1. Note that the first method (Fig. 8(i)) cannot directly indicate the in-plane C atoms of graphene sheets, since it excludes neither the amorphous C atoms or those with a high curvature on the edges of turbostratic graphene networks, nor the undercoordinated C atoms from carbon chain residues of precursor polymers. While in the second method[98] (Fig. 8(j)), the restraints on the planar C atoms are imposed to better identify the formation of graphitic structures, and the schematic is given on the bottom right of Fig. 8. In both Fig. 8(i) and (j), PAN/CL has the fastest conversion ratio to sp^2 C atoms in the early stage of the carbonization and the highest yield of sp^2 C atoms during the standard and extended carbonization processes, disregarding the methods being utilized. PAN/nylon and PAN vary nearly synchronously throughout the entire carbonization. At 8250 ps, PAN, oxidized PAN, and PAN/nylon show approximately identical ratios of sp^2 C atoms, slightly lower than those of PAN/CL. These results also accommodate the C–C distributions of 6-membered all-carbon rings shown in Fig. S7.

From the above analyses, we have demonstrated that PAN/ CL could act as a desired low-cost alternative for PAN-based blend precursors. Which, its carbon content and ring formation analysis indicate a high carbon yield with considerable all-carbon ring cluster growth within a relatively short carbonization time. In addition, the evolutions of O- and N-containing species confirm the functionalities of O- and N-containing groups and explain the distinct behaviors of various PAN-based blend precursors. Furthermore, we select four representative precursors, PAN, oxidized PAN, PAN/CL, and PAN/nylon for the structural characterization studies. The mechanical property related characteristics, *i.e.*, the RDFs, the C–C bond length distributions, and the sp^2 C ratio calculations of the four representative precursors are utilized to elaborate the structural features during the cyclization and carbonization processes. Consequently, as the carbonization substantially develops, among

the four representative precursors, PAN/ CL gives the best performance in correlation with the mechanical properties. In particular, it is found that PAN/CL can yield the highest peak intensity in RDFs, a concentration of C–C bond lengths at r^{1st} of 1.42 Å corresponding to the partial C=C bond length of basal plane C atoms in graphene, and the highest sp^2 C ratios disregarding the methods being used. These results together with the experimental measurements indicate the higher crystallinity of a carbonized PAN/CL blend precursor and more extensive growth of the turbostratic graphene structures, making it possible to reduce the final cost of the CF production by incorporating a naturally abundant and environmentally friendly material to PAN and maintaining the resultant mechanical properties.

4. Conclusion

In this work, a series of ReaxFF MD simulations were performed on the carbonization process for ten single and PAN-based blend polymers. We not only analyzed the formation of all-carbon rings and the evolutions of O-containing and N-containing species, but also conducted structural characterizations with regard to the growth and development of all-carbon ring clusters. Based on these simulations and a qualitative comparison of our simulation data with experimental Raman and TEM measurements, together with the fact that CL is an economical and environment-friendly sauce material, we propose PAN/CL as the most promising cost-effective CF precursor among the considered precursors. In order to substantiate this hypothesis, we first conducted analyses in terms of all-carbon ring formation and functional group evolutions. It was found that PAN/CL remarkably increases the carbon yield with considerable all-carbon ring structure formation. Its carbon conversion to 6-membered all-carbon rings is increased by ~33.3% compared to pure PAN and ~14.3% compared to oxidized PAN. From the analysis of O-containing and N-containing gas emissions of PAN/CL, we found that the embedment of CL to the precursor retains more hetero elements in the system, sustaining 6.7% more O and N atoms than the pure CL, hence more expansive growth and faster propagation of graphitic structures. By examining the carbonization pathways, we identified that the acetals from PAN/CL could transform the C atoms from both PAN and CL to turbostratic graphene or graphitic structure, whereas those of PAN/ PBO mostly transform the C atoms from PBO, resulting in a higher conversion ratio to all-carbon rings of PAN/CL than that of PAN/PBO. The ReaxFF structural characterizations of PAN/CL, such as the enhanced carbon content and turbostratic graphene C conversion, the prominent intensities presented in RDFs and C–C bond length distributions, and the increased sp^2 C ratios computed by two methods all demonstrate the highest crystallinity of carbonized PAN/CL among all the considered precursors. The highest crystallinity can be also observed in ReaxFF trajectories by comparing the morphological variations of all-carbon ring structures over the carbonizing precursors, where more widespread layer-by-layer turbostratic and graphitic structures of PAN/CL can be notably seen when the carbonization time is sufficiently long, up to a few nanoseconds, despite small nanopores possibly coexisting with the carbon structure. The experimental Raman spectra further confirm the highest crystallinity of carbonized PAN/CL, for it shows the lowest I_D/I_G value of 1.06 over all the samples.

Therefore, we recommend PAN/CL or PAN/CL-derived precursors as suitable alternative

cost-effective CF precursors. Such blend precursors not only reduce the final cost of CF production by introducing a naturally abundant and sustainable source without needing an oxidation treatment, but also exhibit increased crystallinity during carbonization, which will likely improve the resultant mechanical properties in applications.

Acknowledgements

Q. M., M. K. and A. C. T. v. D. acknowledge the support from the U. S. Department of Energy (DoE), Vehicle Technologies Office, under Contract Number DE-EE0008195. J. Z. acknowledges the partial financial support by the DoE, Office of Science, Basic Energy Science, Material Science and Engineering. Computations for this research were performed on the PSU's Institute for Cyber Science Advanced Cyber Infrastructure (ICS-ACI).

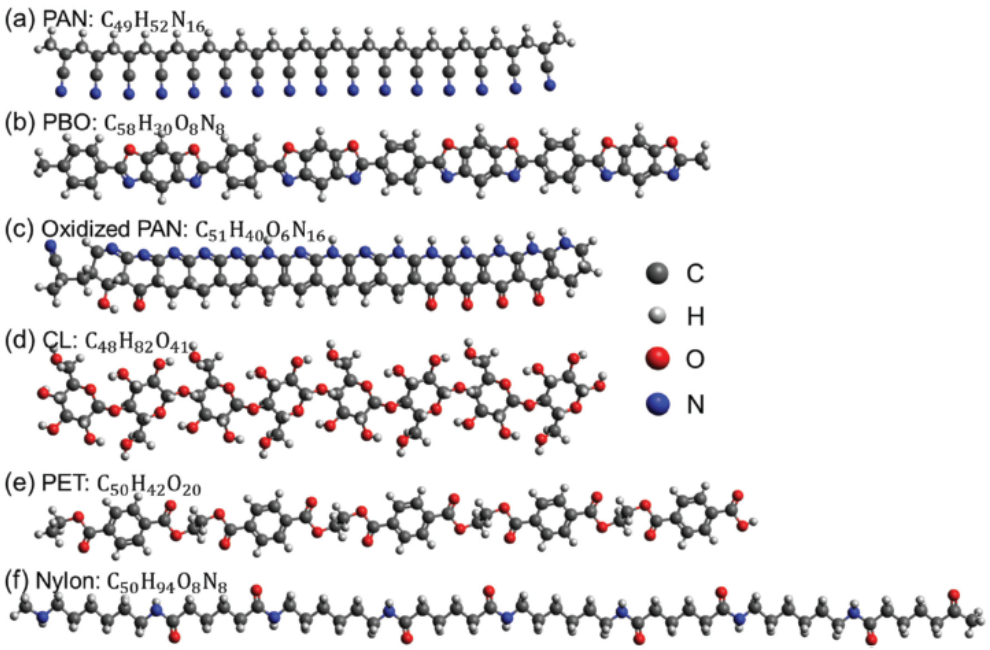

Fig. 1 Molecular structures for building single and blend precursors: (a) PAN, (b) PBO, (c) proposed oxidized PAN,[66,70] (d) CL, (e) PET, (f) nylon. The gray, white, red, and blue spheres represent the carbon, hydrogen, oxygen, and nitrogen atoms, respectively.

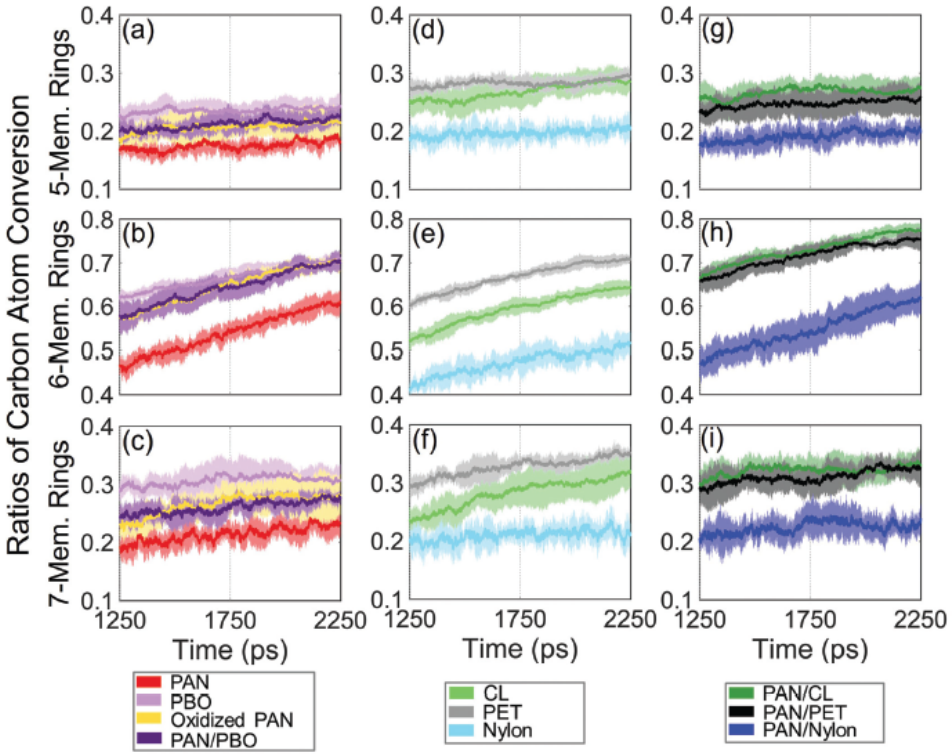

Fig. 2 Evolutions of the normalized all-carbon rings of single and blend precursors over the last 1000 ps of carbonization: (a), (d), and (g) 5-membered all-carbon rings; (b), (e), and (h) 6-membered all-carbon rings; (c), (f), and (i) 7-membered all-carbon rings. The solid dark curves represent the mean values averaged from 6 samples, and the transparent light shadows represent the associated standard deviations from each case.

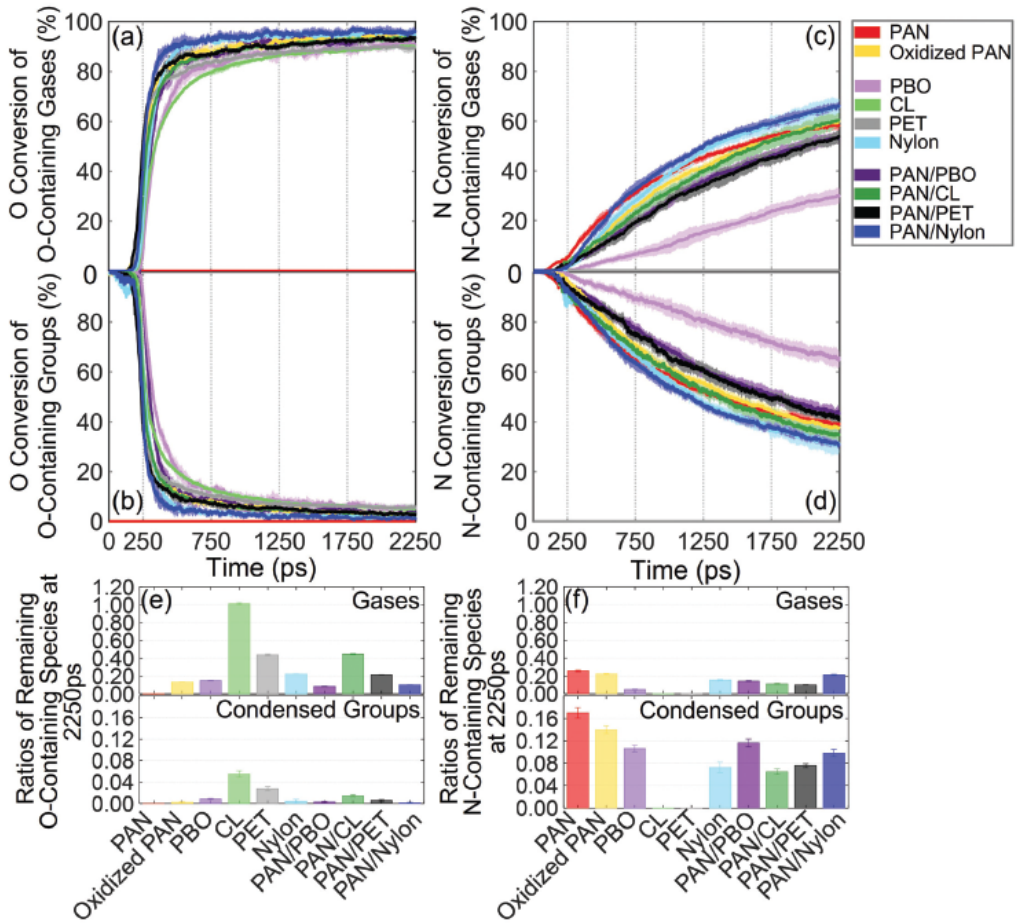

Fig. 3 Evolutions of normalized O- and N-containing species in percentage during heating and carbonization processes: O conversion of (a) O-containing gases and (b) O-containing groups, N conversion of (c) N-containing gases and (d) N-containing groups for all considered single and blend precursors. The solid dark curves represent the mean values averaged from 6 samples, and the light transparent shadows represent the associated standard deviations from each case. The ratios of the remaining O- and N-containing species at the end of carbonization process (2250 ps): (e) O-containing gases and groups, (f) N-containing gases and groups for all considered single and blend precursors. The error bars represent the standard deviations calculated by 6 samples for each case.

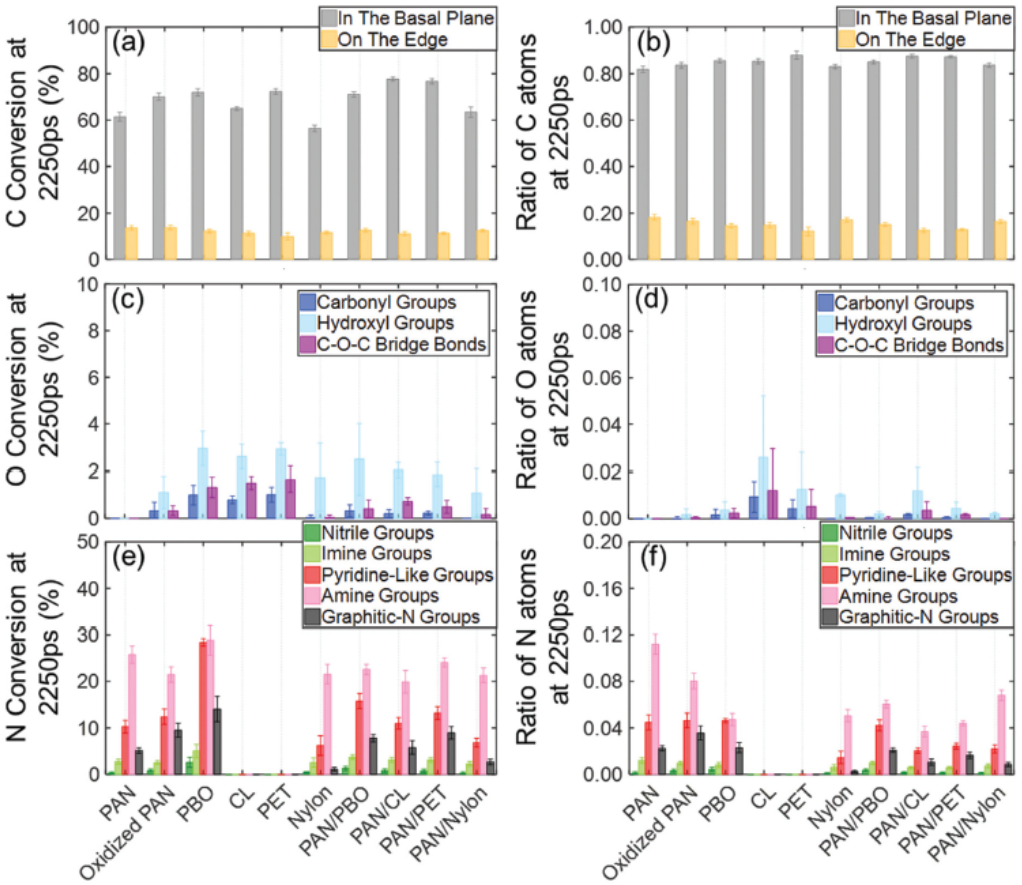

Fig. 4 The growth of all-carbon rings in response to O- and N-containing groups for all considered single and blend precursors at the end of carbonization (t = 2250 ps): (a) percentages and (b) ratios of C atoms converting to basal plane and edge C atoms of turbostratic graphene; (c) percentages and (d) ratios of O atoms converting to carbonyl groups, hydroxyl groups, and C–O–C bridge bonds; (e) percentages and (f) ratios of N atoms converting to nitrile groups, imine groups, pyridine-like groups, amine groups, and graphitic-N groups. The error bars represent the standard deviations calculated by 6 samples for each case.

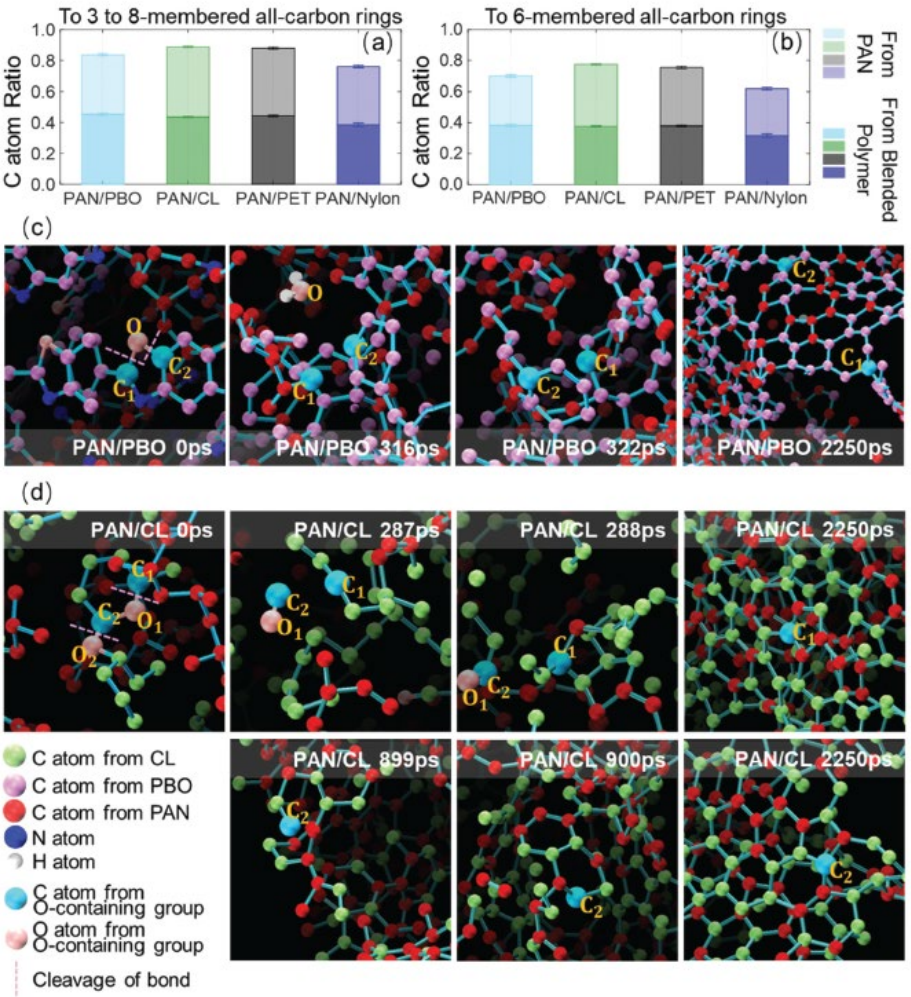

Fig. 5 The fraction of graphitic C atoms originated from PAN or from the blended polymers: (a) the graphitic structures in the form of 3 to 8-membered and (b) 6-membered all-carbon rings. The error bars represent the standard deviations calculated by 6 samples for each case. The comparison of the functionalities of O-containing groups between PAN/PBO and PAN/CL blend precursors: The proposed mechanism of C atoms from (c) PBO and PAN evolving into all-carbon ring structures for the PAN/PBO blend precursor and from (d) CL and PAN evolving into all-carbon ring structures for the PAN/CL blend precursor.

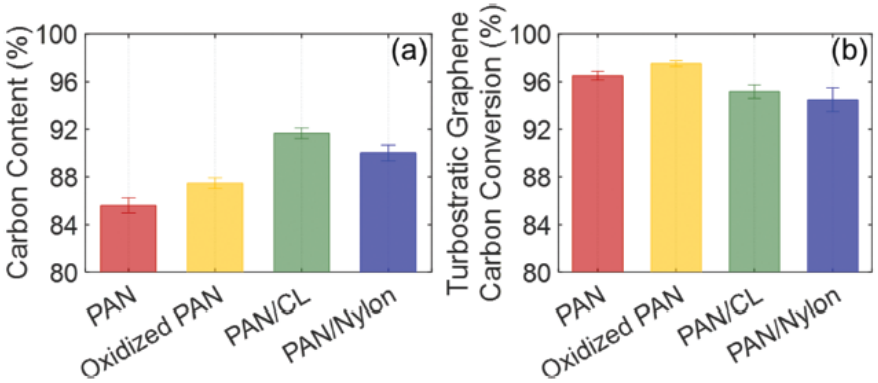

Fig. 6 The carbon conversion analyses of the four representative precursors of interest, PAN, oxidized PAN, PAN/CL, and PAN/nylon: (a) carbon content and (b) turbostratic graphene carbon conversion in percentage from ReaxFF MD simulations.

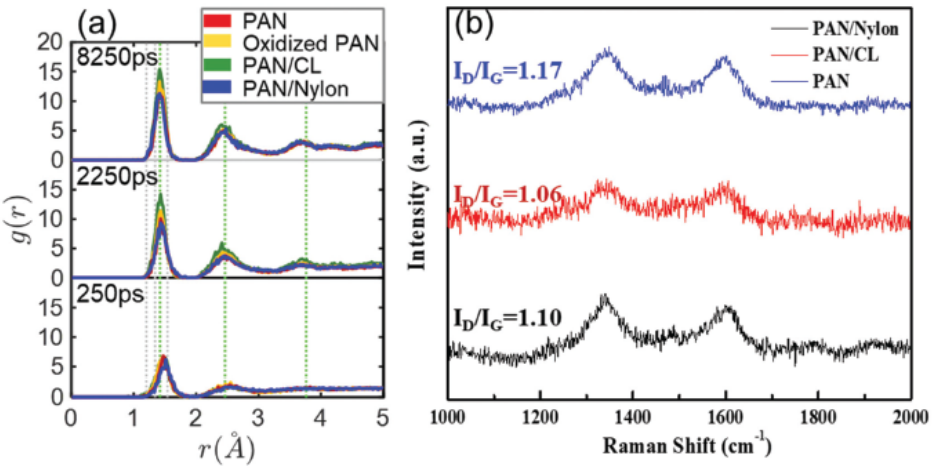

Fig. 7 The C–C pair RDF plots and the Raman spectra of the representative precursors of interest. (a) The C–C pair RDF of PAN, oxidized PAN, PAN/CL, and PAN/nylon carbonized at 2800 K at 250 ps, 2250 ps, and 8250 ps from ReaxFF MD simulations. The three green dot lines from left to right represent the distances between the target C atom and its 1st, 2nd, and 3rd neighbor C atoms from a perfect graphene sheet, which are 1.42 Å, 2.46 Å, and 3.76 Å, respectively (see the schematic in Fig. S6†). The three gray dot lines form left to right represent the bond lengths of triple bonded, double bonded, and single bonded C–C bonds, which are equal to 1.20 Å, 1.34 Å, and 1.54 Å, respectively. (b) The Raman spectra of PAN, PAN/CL, and PAN/nylon carbonized at 1500 °C from experiment.

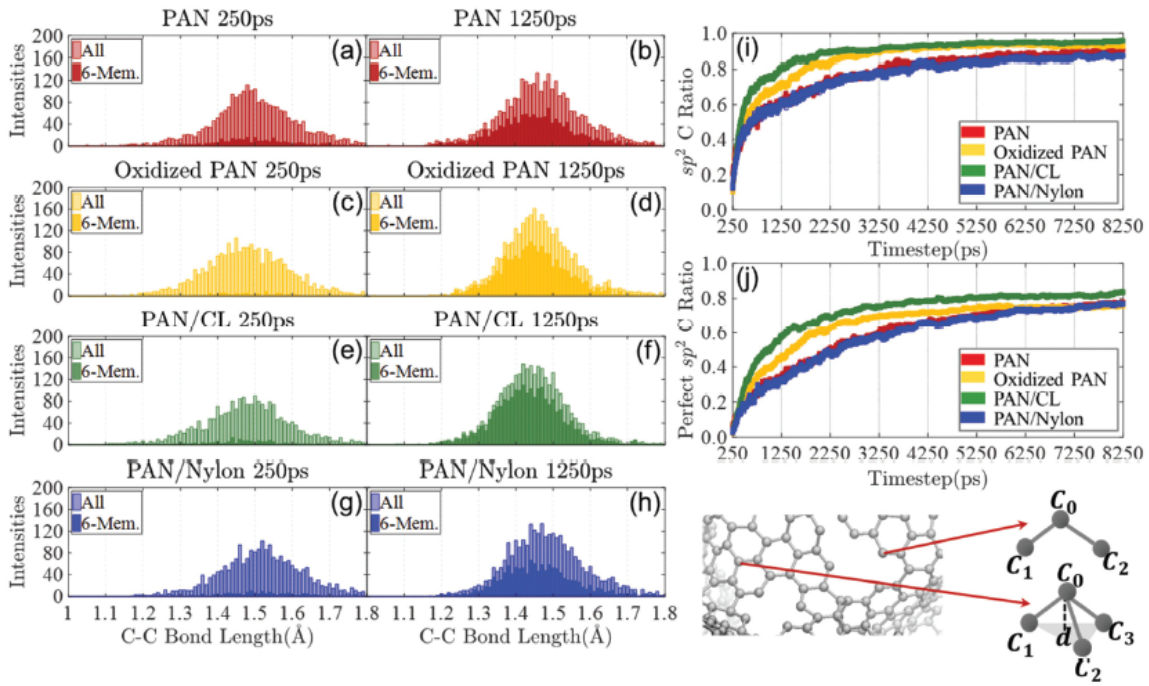

Fig. 8 The C–C bond length distributions evolved during carbonization for the four representative precursors of interest: (a) PAN at 250 ps, (b) PAN at 1250 ps, (c) oxidized PAN at 250 ps, (d) oxidized PAN at 1250 ps, (e) PAN/CL at 250 ps, (f) PAN/CL at 1250 ps, (g) PAN/nylon at 250 ps, (h) PAN/nylon at 1250 ps. The solid color histograms represent the C–C bonds forming the 6-membered all-carbon rings (labeled as "6-Mem."), and the transparent histograms represent the 3 to 8-membered all-carbon rings (labeled as "All"). The calculations of sp^2 C atom hybridization with different methods yield: (i) the ratio of sp^2 C atom hybridization, (j) the ratio of perfect sp^2 C atom hybridization for the four representative precursors of interest.

References

1. High-Performance Structural Fibers for Advanced Polymer Matrix Composites, 2005, DOI: 10.17226/11268.
2. S. Chand, Review carbon fibers for composites, J. Mater. Sci., 2000, 35(6), 1303–1313.
3. X. Huang, Fabrication and properties of carbon fibers, Materials, 2009, 2(4), 2369–2403.
4. D. D. L. Chung, Carbon Fiber Composites, 2012. DOI:10.1016/C2009-0-26078-8.
5. E. Frank, F. Hermanutz and M. R. Buchmeiser, Carbon Fibers: Precursors, Manufacturing, and Properties, Macromol. Mater. Eng., 2012, 297, 493–501.
6. Y. Zhang, N. Tajaddod, K. Song and M. L. Minus, Low temperature graphitization of interphase polyacrylonitrile (PAN), Carbon, 2015, 91, 479–493.
7. D. Choi, H. S. Kil and S. Lee, Fabrication of low-cost carbon fibers using economical precursors and advanced processing technologies, Carbon, 2019, 142, 610–649.
8. A. L. Compere, W. L. Griffith, C. F. Leitten and J. T. Shaffer, Low cost carbon fiber from renewable resources, in International SAMPE Technical Conference, 2001.
9. S. Kubo and J. F. Kadla, Lignin-based Carbon Fibers: Effect of Synthetic Polymer Blending on Fiber Properties, J. Polym. Environ., 2005, 13, 97–105.
10. J. Lin, et al., Improvement of mechanical properties of softwood lignin-based carbon fibers, J. Wood Chem. Technol., 2014, 34, 111–121.
11. E. Svinterikos and I. Zuburtikudis, Carbon nanofibers from renewable bioresources (lignin) and a recycled commodity polymer [poly(ethylene terephthalate)], J. Appl. Polym. Sci., 2016, 133, 43936.
12. M. A. Hunt, T. Saito, R. H. Brown, A. S. Kumbhar and K. Naskar, Patterned functional carbon fibers from polyethylene, Adv. Mater., 2012, 24, 2386–2389.
13. H. Shaikh, et al., Progress in Carbon Fiber and Its Polypropylene- and Polyethylene-Based Composites, Polym. Plast. Technol. Eng., 2014, 53, 1845–1860.
14. I. Karacan and H. Meşeli, Characterization of amorphous carbon fibers produced from thermally stabilized polyamide 6 fibers, J. Ind. Text., 2018, 47(6), 1185– 1211.
15. Y. D. Andrichenko and T. V. Druzhinina, Fabrication of metal-containing carbon fibre based on modified polycarproamide fibre, Fibre Chem., 1999, 31(1), 1–7.
16. X. Zhang, Y. Lu, H. Xiao and H. Peterlik, Effect of hot stretching graphitization on the structure and mechanical properties of rayon-based carbon fibers, J. Mater. Sci., 2014, 49, 673–684.
17. H. Xiao, Y. Lu, W. Zhao and X. Qin, A comparison of the effect of hot stretching on microstructures and properties of polyacrylonitrile and rayon-based carbon fibers, J. Mater. Sci., 2014, 49, 5017–5029.
18. B. A. Newcomb, Processing, structure, and properties of carbon fibers, Composites, Part A, 2016, 91, 262–282.
19. H. C. Liu, A. T. Chien, B. A. Newcomb, Y. Liu and S. Kumar, Processing, Structure, and Properties of Lignin- and CNT-Incorporated Polyacrylonitrile-Based Carbon Fibers, ACS Sustainable Chem. Eng., 2015, 3, 1943–1954.
20. D. K. Seo, J. P. Jeun, H. B. Kim and P. H. Kang, Preparation and characterization of the carbon nanofiber mat produced from electrospun pan/lignin precursors by electron beam irradiation, Rev. Adv. Mater. Sci., 2011, 28, 31–34.
21. J. M. Spörl, et al., Cellulose-Derived Carbon Fibers with Improved Carbon Yield and Mechanical Properties, Macromol. Mater. Eng., 2017, 302, 1700195.

22. A. A. Ogale, M. Zhang and J. Jin, Recent advances in carbon fibers derived from biobased precursors, J. Appl. Polym. Sci., 2016, 133(45), 43794.
23. D. S. Achilias, E. Antonakou, C. Roupakias, P. Megalokonomos and A. Lappas, Recycling techniques of polyolefins from plastic wastes, Global NEST J., 2008, 10, 114–122.
24. K. W. Kim, et al., Preparation and thermal properties of polyethylene-based carbonized fibers, Carbon Lett., 2015, 16, 62–66.
25. P. Goulis, G. Konstantopoulos, I. A. Kartsonakis, et al., Thermal Treatment of Melt-Spun Fibers Based on High Density PolyEthylene and Lignin, C, 2017, 3, 35.
26. S. Chen, Z. Liu, S. Jiang and H. Hou, Carbonization: A feasible route for reutilization of plastic wastes, Sci. Total Environ., 2020, 710, 136250.
27. J. W. Kim and J. S. Lee, Preparation of carbon fibers from linear low density polyethylene, Carbon, 2015, 94, 524–530.
28. E. J. Hukkanen, et al., A novel continuous multiphase reactor for chemically processing polymer fibers, Ind. Eng. Chem. Res., 2018, 57, 6123–6130.
29. B. E. Barton, et al., High-Modulus Low-Cost Carbon Fibers from Polyethylene Enabled by Boron Catalyzed Graphitization, Small, 2017, 13, 1–7.
30. G. S. Wortberg, A. De Palmenaer, M. Beckers, G. Seide and T. Gries, Polyethylene-based carbon fibers by the use of sulphonation for stabilization, Fibers, 2015, 3, 373–379.
31. B. E. Barton, et al., The chemical transformation of hydrocarbons to carbon using SO3 sources, Carbon, 2015, 94, 465–471.
32. S. Bourbigot, X. Flambard and S. Duquesne, Thermal degradation of poly(p-phenylenebenzobisoxazole) and poly(p-phenylenediamine terephthalamide) fibres, Polym. Int., 2001, 50(1), 157–164.
33. L. Zhang, et al., Converting PBO fibers into carbon fibers by ultrafast carbonization, Carbon, 2020, 159, 432–442.
34. Q. Mao, S. Rajabpour, M. Kowalik and A. C. T. van Duin, Predicting cost-effective carbon fi ber precursors: Unraveling the functionalities of oxygen and nitrogen-containing groups during carbonization from ReaxFF simulations, Carbon, 2020, 159, 25–36.
35. J. A. Newell, D. K. Rogers, D. D. Edie and C. C. Fain, Direct carbonization of PBO fiber, Carbon, 1994, 32, 651–658.
36. J. A. Newell, D. D. Edie and E. L. Fuller, Kinetics of carbonization and graphitization of PBO fiber, J. Appl. Polym. Sci., 1996, 60, 825–832.
37. Y. Kaburagi, K. Yokoi, A. Yoshida and Y. Hishiyama, Highly graphitized carbon fiber prepared from poly (p-phenylene-benzo-bis-oxazole) fiber, Tanso, 2005, 2005, 111–114.
38. H. G. Chae and S. Kumar, Rigid-rod polymeric fibers, J. Appl. Polym. Sci., 2006, 100, 791–802.
39. O. Hosseinaei, D. P. Harper, J. J. Bozell and T. G. Rials, Improving processing and performance of pure lignin carbon fibers through hardwood and herbaceous lignin blends, Int. J. Mol. Sci., 2017, 18, 1410.
40. H. C. Liu, et al., Polyacrylonitrile sheath and polyacrylonitrile/lignin core bi-component carbon fiber, Carbon, 2019, 149, 165–172.
41. S. Vincent, et al., Regenerated Cellulose and Willow Lignin Blends as Potential Renewable Precursors for Carbon Fibers, ACS Sustainable Chem. Eng., 2018, 6, 5903–5910.
42. J. Mikkilä, et al., Fungal Treatment Modifies Kraft Lignin for Lignin- And Cellulose-

Based Carbon Fiber Precursors, ACS Omega, 2020, 5, 6130–6140.
43. J. Zhu, et al., A sustainable platform of lignin: From bioresources to materials and their applications in rechargeable batteries and supercapacitors, Prog. Energy Combust. Sci., 2020, 76, 100788.
44. A. Milbrandt and S. Booth, Carbon Fiber from Biomass, Clean Energy Manuf. Anal. Cent., 2016, pp. 1–27.
45. H. C. Liu, A. T. Chien, B. A. Newcomb, A. A. B. Davijani and S. Kumar, Stabilization kinetics of gel spun polyacrylonitrile/lignin blend fiber, Carbon, 2016, 101, 382–389.
46. R. Zhang, et al., Unlocking the response of lignin structure for improved carbon fiber production and mechanical strength, Green Chem., 2019, 21, 4981–4987.
47. H. Chang, et al., Carbon fibers from polyacrylonitrile/cellulose nanocrystal nanocomposite fibers, Carbon, 2019, 145, 764–771.
48. X. Dong, et al., Polyacrylonitrile/lignin sulfonate blend fiber for low-cost carbon fiber, RSC Adv., 2015, 5, 42259–42265.
49. J. Jin and A. A. Ogale, Carbon fibers derived from wet-spinning of equi-component lignin/polyacrylonitrile blends, J. Appl. Polym. Sci., 2018, 135, 1–9.
50. Y. S. Tay, M. Liu, J. S. K. Lim, H. Chen and X. Hu, Phthalonitrile prepolymer and PAN blends: New strategy for precursor stabilization and pyrolytic char yield enhancement, Polym. Degrad. Stab., 2020, 172, 109056.
51. E. Jiang, et al., Influence of Different Nanocellulose Additives on Processing and Performance of PAN-Based Carbon Fibers, ACS Omega, 2019, 4, 9720–9730.
52. S. P. Maradur, et al., Preparation of carbon fibers from a lignin copolymer with polyacrylonitrile, Synth. Met., 2012, 162, 453–459.
53. H. Kim, R. Jalili, G. M. Spinks, G. G. Wallace and S. Jeong, High-strength graphene and polyacrylonitrile composite fiber enhanced by surface coating with polydopamine, Compos. Sci. Technol., 2017, 149, 280–285.
54. M. Kowalik, et al., Atomistic Scale Analysis of the Carbonization Process for C/H/O/N-Based Polymers with the ReaxFF Reactive Force Field, J. Phys. Chem. B, 2019, 123, 5357–5367.
55. A. C. T. van Duin, S. Dasgupta and F. Lorant, ReaxFF: A Reactive Force Field for Hydrocarbons, J. Phys. Chem. A, 2001, 105, 9396–9409.
56. T. Liang, et al., Reactive potentials for advanced atomistic simulations, Annu. Rev. Mater. Res., 2013, 43, 109–129.
57. K. Chenoweth, A. C. T. van Duin, S. Dasgupta and W. A. Goddard III, Initiation mechanisms and kinetics of pyrolysis and combustion of JP-10 hydrocarbon jet fuel, J. Phys. Chem. A, 2009, 113(9), 1740–1746.
58. J. Liu and X. Guo, ReaxFF, molecular dynamics simulation of pyrolysis and combustion of pyridine, Fuel Process. Technol., 2017, 161, 107–115.
59. S. Arvelos, O. A. Jr and C. E. Hori, Journal of Analytical and Applied Pyrolysis ReaxFF molecular dynamics study on the pyrolysis process of cyclohexanone, J. Anal. Appl. Pyrolysis, 2019, 141, 104620.
60. F. Xu, et al., ReaxFF-based molecular dynamics simulation of the initial pyrolysis mechanism of lignite, Fuel Process. Technol., 2019, 195, 106147.
61. M. Gao, X. Li, C. Ren, Z. Wang, Y. Pan and L. Guo, Construction of a multicomponent molecular model of Fugu coal for ReaxFF-MD pyrolysis simulation, Energy Fuels, 2019, 33(4), 2848–2858.

62. K. Chenoweth, A. C. T. van Duin and W. A. Goddard III, ReaxFF reactive force field for molecular dynamics simulations of hydrocarbon oxidation, J. Phys. Chem. A, 2008, 112(5), 1040–1053.
63. C. Ashraf, A. Jain, Y. Xuan and A. C. T. van Duin, ReaxFF based molecular dynamics simulations of ignition front propagation in hydrocarbon/oxygen mixtures under high temperature and pressure conditions, Phys. Chem. Chem. Phys., 2017, 19(7), 5004–5017.
64. C. Ashraf and A. C. T. van Duin, Extension of the ReaxFF combustion force field toward syngas combustion and initial oxidation kinetics, J. Phys. Chem. A, 2017, 121(5), 1051–1068.
65. H. Kwon, S. Shabnam, A. C. T. van Duin and Y. Xuan, Numerical simulations of yield-based sooting tendencies of aromatic fuels using ReaxFF molecular dynamics, Fuel, 2020, 262, 116545.
66. B. Saha, Y. Dzenis and G. C. Schatz, Multi-step mechanism of carbonization in templated polyacrylonitrile derived fibers: ReaxFF model uncovers origins of graphite alignment, Carbon, 2015, 94, 694–704.
67. S. Rajabpour, et al., Low-temperature carbonization of polyacrylonitrile/graphene carbon fibers: A combined ReaxFF molecular dynamics and experimental study, Carbon, 2021, 174, 345–356.
68. J. Zhu, et al., Unveiling Carbon Ring Structure Formation Mechanisms in Polyacrylonitrile-Derived Carbon Fibers, ACS Appl. Mater. Interfaces, 2019, 11, 42288–42297.
69. Z. Gao, et al., Graphene reinforced carbon fibers, Sci. Adv., 2020, 6, 1–11.
70. K. Morita, Y. Murata, A. Ishitani, K. Murayama, T. Ono and Nakajima, Characterization of commercially available PAN (polyacrylonitrile)-based carbon fibers, Pure Appl. Chem., 1986, 58(3), 455–468.
71. Y. Nishiyama, P. Langan and H. Chanzy, Crystal Structure and Hydrogen-Bonding System in Cellulose I from Synchrotron X-ray and Neutron Fiber Diffraction, J. Am. Chem. Soc., 2002, 124(31), 9074–9082.
72. Q. Mao, et al., Interface Strain Induced Hydrophobic Facet Suppression in Cellulose Nanocomposite Embedded with Highly Oxidized Monolayer Graphene Oxide, Adv. Mater. Interfaces, 2017, 4, 1–11.
73. S. D. Mustafov, A. K. Mohanty, M. Misra and M.Ö Seydibeyoğlu, Fabrication of conductive Lignin/PAN carbon nanofiber with enhanced graphene for the modified electrode, Carbon, 2019, 147, 262–275.
74. O. Zabihi, S. Shafei, S. M. Fakhrhoseini, M. Ahmadi, H. A. Nazarloo, R. Stanger, M. Naebe, et al., Low-cost carbon fibre derived from sustainable coal tar pitch and polyacrylonitrile: fabrication and characterisation, Materials, 2019, 12(8), 1281.
75. T. Ko, The Influence of Pyrolysis on Physical Properties and Microstructure of Modified PAN Fibers during Carbonization, J. Appl. Polym. Sci., 1991, 43, 589–600.
76. H. Khayyam, et al., PAN precursor fabrication, applications and thermal stabilization process in carbon fiber production: Experimental and mathematical modelling, Prog. Mater. Sci., 2020, 107, 100575.
77. H. Liu, et al., Preparation, stabilization and carbonization of a novel polyacrylonitrile-based carbon fiber precursor, Polymers, 2019, 11, 1150.
78. S. Nunna, M. Maghe, S. M. Fakhrhoseini, B. Polisetti and M. Naebe, A pathway to reduce energy consumption in the thermal stabilization process of carbon fiber

production, Energies, 2018, 11, 1145.
79. G. Golkarnarenji, et al., Production of low cost carbon-fiber through energy optimization of stabilization process, Materials, 2018, 11, 1–13.
80. S. Arbab and A. Zeinolebadi, Quantitative analysis of the effects of comonomers and heating conditions on the stabilization reactions of polyacrylonitrile fibers as carbon fiber precursors, Polym. Degrad. Stab., 2017, 139, 107–116.
81. D. A. Baker and T. G. Rials, Recent advances in low-cost carbon fiber manufacture from lignin, J. Appl. Polym. Sci., 2013, 130, 713–728.
82. P. Bajpai, Carbon Fibre from Lignin, 2017.
83. A. Bengtsson, et al., Carbon Fibers from Lignin-Cellulose Precursors: Effect of Carbonization Conditions, ACS Sustainable Chem. Eng., 2020, 8, 6826–6833.
84. J. F. Kadla, et al., Lignin-based carbon fibers for composite fiber applications, Carbon, 2002, 40, 2913–2920.
85. N. Byrne, R. De Silva, Y. Ma, H. Sixta and M. Hummel, Enhanced stabilization of cellulose-lignin hybrid filaments for carbon fiber production, Cellulose, 2018, 25, 723–733.
86. T. A. Adegbola, O. Agboola and O. S. I. Fayomi, Review of polyacrylonitrile blends and application in manufacturing technology: recycling and environmental impact, Results Eng., 2020, 7, 100144.
87. Z. Cao, W. Li, X. Suo, Y. Liu and C. Lu, Structures and cyclization behaviors of gel-spun cellulose/polyacrylonitrile composite fibers, Polym. Test., 2020, 81, 106276.
88. X. Jiang, Q. Ouyang, D. Liu, J. Huang, H. Ma, Y. Chen, W. Sun, et al., Preparation of low-cost carbon fiber precursors from blends of wheat straw lignin and commercial textile-grade polyacrylonitrile (PAN), Holzforschung, 2018, 72(9), 727–734.
89. S. Devadas, et al., Fabrication and characterization of electrospun poly(Acrylonitrile-co-methyl acrylate)/lignin nanofibers: Effects of lignin type and total polymer concentration, Polymers, 2021, 13, 992.
90. M.Ö Seydibeyolu, A novel partially biobased pan-lignin blend as a potential carbon fiber precursor, J. Biomed. Biotechnol., 2012, 598324.
91. K. Joshi, M. I. Arefev and L. V. Zhigilei, Generation and characterization of carbon fi ber microstructures by atomistic simulations, Carbon, 2019, 152, 396–408.
92. E. M. D. J. Fitzer and D. J. Müller, The influence of oxygen on the chemical reactions during stabilization of pan as carbon fiber precursor, Carbon, 1975, 13(1), 63–69.
93. J. Luo, H. Chang, P. H. Wang, R. J. Moon and S. Kumar, Cellulose nanocrystals effect on the stabilization of polyacrylonitrile composite films, Carbon, 2018, 134, 92–102.
94. J. Luo, et al., Influence of high loading of cellulose nanocrystals in polyacrylonitrile composite films, Cellulose, 2017, 24, 1745–1758.
95. J. Zhu, S. W. Park, H.-I. Joh, H. C. Kim and S. Lee, Preparation and characterization of isotropic pitch-based carbon fiber, Carbon Lett., 2013, 14, 94–98.
96. J. Zhu, et al., Nitrogen-doped carbon nanofibers derived from polyacrylonitrile for use as anode material in sodium-ion batteries, Carbon, 2015, 94, 189–195.
97. S.-J. Park, Carbon Fibers, 2nd edn, 2018.
98. K. Li, et al., ReaxFF Molecular Dynamics Simulation for the Graphitization of Amorphous Carbon: A Parametric Study, J. Chem. Theory Comput., 2018, 14, 2322–2331.